Elsevier Editorial System(tm) for Micron
Manuscript Draft

Manuscript Number: JMIC-D-13-00193R1

Title: Site-specific ionisation edge fine-structure of Rutile in the electron microscope

Article Type: SI: David C.H. Cockayne SI

Keywords: EELS; Channelling; ELCE

Corresponding Author: Mr. Walid Hetaba,

Corresponding Author's Institution: Vienna University of Technology

First Author: Walid Hetaba

Order of Authors: Walid Hetaba; Stefan Löffler; Marc-Georg Willinger; Manfred E Schuster; Robert Schlögl; Peter Schattschneider

Abstract: Combined Bloch-wave and density functional theory simulations are performed to investigate the effects of different channelling conditions on the fine-structure of electron energy-loss spectra. The simulated spectra compare well with experiments. Furthermore, we demonstrate that using this technique, the site-specific investigation of atomic orbitals is possible. This opens new possibilities for chemical analyses.

Highlights (for review)

We used 2 simulation programs to calculate the site-specific fine-structure of Rutile.

Comparing simulations and experiments the very good agreement is evident.

We are able to study the influence of atomic orbitals using channelling effects.

*Manuscript
Click here to view linked References

Site-specific ionisation edge fine-structure of Rutile in the electron microscope

Walid Hetaba[a,b,*], Stefan Löffler[a], Marc-Georg Willinger[c], Manfred Erwin Schuster[c], Robert Schlögl[c], Peter Schattschneider[a,d]

[a] *University Service Centre for Transmission Electron Microscopy, Vienna University of Technology, Wiedner Hauptstrasse 8-10, A-1040 Wien, Austria*
[b] *Thin Films and Physics of Nanostructures, Department of Physics, Bielefeld University, Universitätsstrasse 25, D-33615 Bielefeld, Germany*
[c] *Department of Inorganic Chemistry, Fritz-Haber-Institut der Max-Planck-Gesellschaft, Faradayweg 4-6, D-14195 Berlin, Germany*
[d] *Institute of Solid State Physics, Vienna University of Technology, Wiedner Hauptstrasse 8-10, A-1040 Wien, Austria*

Abstract

Combined Bloch-wave and density functional theory simulations are performed to investigate the effects of different channelling conditions on the fine-structure of electron energy-loss spectra. The simulated spectra compare well with experiments. Furthermore, we demonstrate that using this technique, the site-specific investigation of atomic orbitals is possible. This opens new possibilities for chemical analyses.

Keywords: EELS, Channelling, ELCE

1. Introduction

In 1982, Taftø and Spence first combined electron channelling with analytical transmission electron microscopy (TEM) (Taftø and Spence, 1982). They called the technique *Atom Location by Channelling Enhanced Microanalysis* (ALCHEMI) (Spence and Taftø, 1983) and used it to identify crystallographic sites of atomic species and to analyse impurities. This was done by using the dependence of the characteristic X-ray emission on the orientation of the incident electron beam with respect to the sample when doing energy dispersive X-Ray (EDX) analyses. Since these first experiments, ALCHEMI has been used frequently in analytical microscopy. Soon after the first ALCHEMI experiments, electron channelling was also used in connection with electron energy-loss spectrometry (EELS) (Taftø and Krivanek, 1982). This technique is called *Energy Loss by Channelled Electrons* (ELCE) (Krivanek et al., 1982).

*Corresponding author at: University Service Centre for Transmission Electron Microscopy, Vienna University of Technology, Wiedner Hauptstrasse 8-10, A-1040 Wien, Austria
Email address: walid.hetaba@tuwien.ac.at (Walid Hetaba)

The principle of both ALCHEMI and ELCE techniques is rather simple. The probe electrons in the crystal can be described as Bloch-waves (Kittel, 2006; Williams and Carter, 2009). The Bloch-waves differ, among other things, in the locations of their intensity-maxima. Depending on the orientation of the crystal with respect to the electron beam (described by the excitation error), these Bloch-waves have different weights. If an atom coincides with these intensity maxima, the energy-loss signal or X-ray signal originating from its site will be enhanced. In a simple picture, channelling conditions for the electron beam can be used to probe site-specific chemical signals. The initial enthusiasm with ELCE faded away rapidly, however, when it was realised that the detailed description proves to be more difficult than one might expect.

ALCHEMI, on the other hand, is easier to perform and to interpret than ELCE. This is because in ALCHEMI, only the incoming electron wave has to be considered. For ELCE, not only the incoming wave but also the outgoing electron wave as well as inelastic and elastic scattering processes have to be considered. As the spectrometer is usually placed off axis in ELCE experiments, long acquisition times are necessary and spectra often show a low signal-to-noise ratio. Due to these theoretical and instrumental shortcomings, ELCE was not widely used until recently (Tatsumi and Muto, 2009).

Usually, measurements are performed under systematic-row conditions in order to have a definite set of Bragg spots excited. This gives rise to a defined set of Bloch-waves. Thus, it is easier to get reproducible experimental conditions which allow to compare theory and measurements more easily. The Bloch-wave intensity distribution in systematic row conditions has been studied extensively by numerous authors (e.g. Williams and Carter, 2009; Nelhiebel, 1999; Hébert et al., 2008). It was found that it is strongly dependent on sample thickness and beam tilt. Hence, numerical simulations for the experimental set of parameters have to be performed to interpret ELCE measurements.

Even though its mathematical description is demanding, the ELCE technique can be used to study the fine-structure of ionisation edges (energy loss near edge structure — ELNES) in more detail to investigate atomic orbitals with site-specificity. Nelhiebel et al. (2000) investigated the fine-structure by choosing a single (high intensity) direction in the diffraction plane. Here, we go beyond this approach. By analysing the differences in the site-specific ionisation edge fine-structure for different detector positions, we are able to probe different orientations of the final orbitals.

2. Simulations

We used Rutile (TiO_2) as a test system because, due to its tetragonal unit cell, it is suitable to investigate the site-specificity of the ionisation edge fine-structure using channelling effects. In Fig. 1, a schematic of the Rutile unit cell is shown. The arrows depict each atom's local coordinate system. The crystallographic structure's space group gives rise to the fact that the local coordinate systems of some of the Oxygen atoms (depicted in yellow) are rotated by 90° with respect to those of the other Oxygen atoms (depicted in red). A

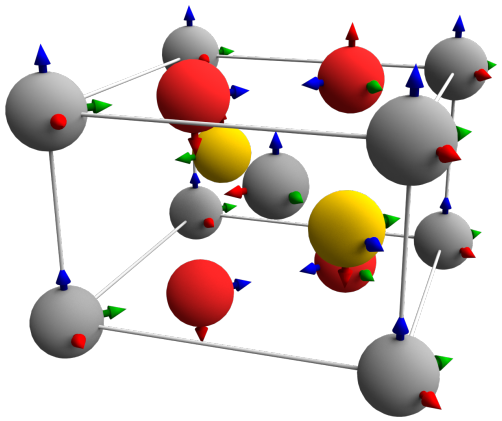

Figure 1: Schematic of the Rutile unit cell. Titanium atoms are plotted in grey while Oxygen atoms are plotted in red and yellow. The arrows depict each atom's local coordinate system due to the structure's symmetry (red: x-axis, green: y-axis, blue: z-axis).

Table 1: Crystallographic data of Rutile (Villars and Calvert, 1996).

Space group	Lattice Parameters	Atom positions
P42/mnm (136)	a = b = 4.59 Å	Ti: (0 0 0)
	c = 2.96 Å	O: (0.3 0.3 0.3)
	$\alpha = \beta = \gamma = 90°$	

detailed description of the bonding situation in Rutile as well as a visualisation using electron density plots is given by Sorantin and Schwarz (1992), where it is shown that the metal atoms in the structure are octahedrally coordinated by anions. Therefore, the Titanium atoms show an e_g–t_{2g} splitting.[1] Due to the hybridisation between Ti and O orbitals, the splitting can also be seen in the Oxygen projected partial density of states (pDOS). This gives rise to the assumption that by using distinct channelling conditions, the influence of different orbitals on the measured energy-loss spectra can be varied. The Oxygen pDOS is plotted in Fig. 2. It was calculated using the density functional theory (DFT) simulation package WIEN2k (Blaha et al., 2001). The calculational details of the unit cell for the calculation can be found in Tab. 1. For the calculation, 1000 k-Points were used and the value for $R_{MT}K_{max}$ was set to 7. The muffin tin radii R_{MT} for the Oxygen and Titanium atoms were chosen to be 1.72 a.u. and 1.94 a.u., respectively.

Due to calculational details[2], in the following work we keep the focus on the Oxygen K-edge (Hetaba et al., 2012; Laskowski and Blaha, 2010).

[1] Although the octahedra are slightly distorted, it is still justified to use the "e_g" and "t_{2g}" classification rather than that of a lower symmetry (Sorantin and Schwarz, 1992).

[2] Using DFT, the calculation of L-edges is not as reliable as that of K-edges (Laskowski and Blaha, 2010).

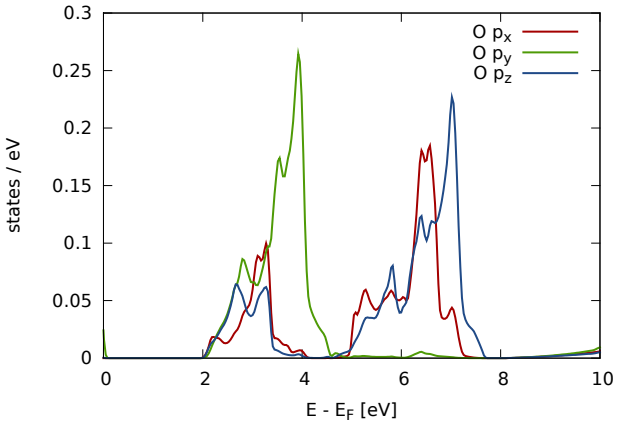

Figure 2: Oxygen projected density of states of Rutile above the Fermi-energy. The calculation was performed using WIEN2k.

We apply a combination of two simulation software packages to calculate the effects of different channelling conditions on the measured Oxygen K-edge electron energy-loss spectra. The first program package uses the Bloch-wave formalism for treating elastic scattering (Löffler and Schattschneider, 2010), while it uses the mixed dynamic form factor (MDFF) (Kohl and Rose, 1985) to describe inelastic scattering events. The double differential scattering cross-section (DDSC) can be calculated as

$$\begin{aligned}\frac{\partial^2\sigma}{\partial E\partial\Omega} &= \frac{4\gamma^2}{a_0^2}\frac{k_f}{k_i}\sum_{\boldsymbol{x}}\sum_{\substack{j,j',l,l'\\ \boldsymbol{g},\boldsymbol{g'},\boldsymbol{h},\boldsymbol{h'}}} \varepsilon_j C^j_{\boldsymbol{g}}(\tilde{\varepsilon}_l\tilde{C}^l_{\boldsymbol{h}})^* \times \\ &\quad (\varepsilon_{j'}C^{j'}_{\boldsymbol{g'}})^*\tilde{\varepsilon}_{l'}\tilde{C}^{l'}_{\boldsymbol{h'}}\cdot e^{2\pi i(\boldsymbol{q}-\boldsymbol{q'})\cdot\boldsymbol{x}}\times \\ &\quad e^{2\pi i t(\tilde{\gamma}_{l'}-\tilde{\gamma}_l)}\cdot\frac{S_{\boldsymbol{x}}(\boldsymbol{q},\boldsymbol{q'},E)}{q^2q'^2}\,. \end{aligned} \tag{1}$$

γ is the relativistic factor, a_0 is the Bohr radius, k_f and k_i are the final and the incident wave vectors. The indices $\boldsymbol{g}$, $\boldsymbol{g'}$, $\boldsymbol{h}$ and $\boldsymbol{h'}$ describe vectors in reciprocal space, j, j', l and l' are the Bloch-wave indices, ε is the excitation amplitude, the C are the Bloch coefficients and t is the sample thickness. The $\tilde{\gamma}_l$ and $\tilde{\gamma}_{l'}$ are called *Anpassung*, their derivation can be found in Williams and Carter (2009). All variables with a tilde describe the outgoing electron wave, while all variables without a tilde describe the incoming electron wave. $\boldsymbol{q}$ and $\boldsymbol{q'}$ describe the momentum transfers and $\boldsymbol{x}$ the position of a target atom. All target atoms are summed over incoherently. $S_{\boldsymbol{x}}(\boldsymbol{q},\boldsymbol{q'},E)$ is the mixed dynamic form factor of the atom at position $\boldsymbol{x}$. For more details on this formula, see for example Nelhiebel (1999), Löffler (2013) and Rusz et al. (2013).

Using the program, the distribution of the Bloch-waves inside a crystal can

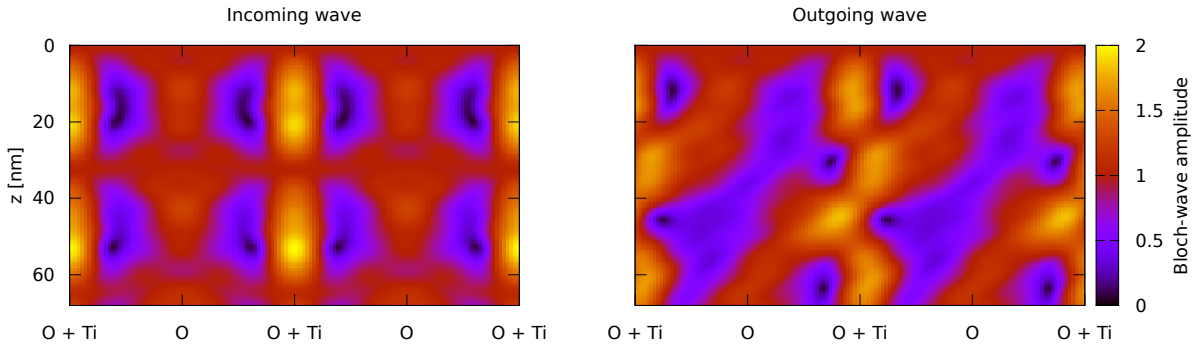

Figure 3: Calculation of the Bloch-wave amplitudes in a 70 nm thick Rutile crystal. The simulations were performed for a specimen that was tilted out of the [1 1 0] zone axis in order to obtain a systematic row condition including the $G = (1\,\bar{1}\,0)$ diffraction spot. The vertical axes correspond to the $(4\,\bar{4}\,0)$ planes. Left: Incoming electron wave. Right: Outgoing electron wave. The detector is at a position displaced from the origin of the diffraction pattern in the direction of G, at a position 1/3 of the distance to this reflection.

be calculated. In Fig. 3 (left), the Bloch-wave distribution of the incoming electron wave in 70 nm thick Rutile in [1 1 0] projection is plotted. In Fig. 3 (right), the Bloch-wave distribution of the outgoing electron wave that reaches the EELS detector is plotted for the same crystal specifications.

One can easily see that for the two electron waves, the amplitude distribution inside the crystal shows quite extensive changes. As the interaction of the beam electrons with the sample happens mainly at the regions in the crystal where the amplitudes have their maxima, interpretation of the measured spectra is not straightforward any more. Therefore, detailed simulations are necessary for measurement interpretation. In order to simulate the effects on the energy-loss spectra caused by these changes of the amplitude distribution, the MDFF has to be calculated.

The MDFF for an atom at the origin can be written as

$$S(\boldsymbol{q}, \boldsymbol{q}', E) = \sum_{i,f} \langle i|e^{i\boldsymbol{q}\boldsymbol{r}}|f\rangle \, \langle f|e^{-i\boldsymbol{q}'\boldsymbol{r}}|i\rangle \, \delta(E_i - E_f - E). \tag{2}$$

Again, $\boldsymbol{q}$ and $\boldsymbol{q}'$ describe the momentum transfers, while the position operator of the target electron is denoted by $\boldsymbol{r}$. The initial state of the target with energy E_i is described by $|i\rangle$ while the final state with energy E_f is referred to as $|f\rangle$ (Schattschneider et al., 2001).

In order to invesitgate the changes in the ionisation edge fine-structure, we use WIEN2k to describe the target's states in the formula above. The MDFF needed in the first simulation package is calculated based on the cross-density of states (XDOS) and the wave functions of the target electron by TELNES.3

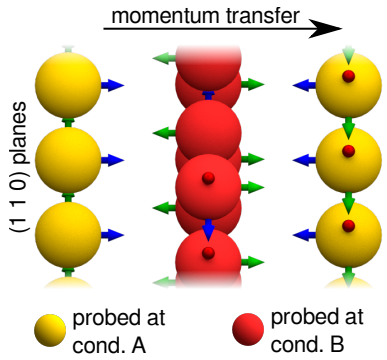

Figure 4: Sketch of the $(1\,\bar{1}\,0)$ planes in the Rutile crystal and the local coordinate systems of the Oxygen atoms (red, green and blue arrows). By using different channelling conditions, different Oxygen columns (red or yellow, respectively) are probed predominantly. In each case, the orbitals parallel to the momentum transfer vector give the dominant contribution. Here, the direction of the momentum transfer vector is chosen such that it illustrates the first example given in the text. For the directions in the actual experiment see Fig. 6.

subroutines implemented in WIEN2k (Nelhiebel et al., 1999; Schattschneider et al., 2006; Rusz et al., 2007).

For the simulations on Rutile shown in this work, the crystallographic data as given in Tab. 1 was used in the input file for the Bloch-wave program. Furthermore, the details of the experimental setup were chosen such that, starting from the $[1\,1\,0]$ zone axis, a systematic row condition including the $(1\,\bar{1}\,0)$ diffraction spot was established. A combination of 5 incoming and 4 outgoing Bloch-waves was used. In order to get a simulation of the Oxygen K-edge energy-loss spectra in the desired energy range of 525 eV to 539 eV, the wave functions of the target electrons and the cross-density of states at a certain energy-loss value has to be extracted from a previous WIEN2k calculation. Then, the DDSCs for this energy-loss value are calculated using the Bloch-wave program. Finally, these steps are repeated until the desired energy-loss range is covered.

When changing the channelling conditions, different colums of Oxygen atoms are probed predominantly (see conditions "A" and "B" in Fig. 4). For dipole allowed transitions in the scattering process, those states that lie parallel to the momentum transfer vector $\boldsymbol{q}$ are probed predominantly, as can be seen from the inner product of the momentum transfer vector and the position operator in the exponential function in equation 2. Thus, by changing either the channelling conditions or the direction of the momentum transfer vector, different orbitals can be probed. In our case, changing the channelling conditions and keeping the momentum transfer vector would result in probing predominantly the orbitals that lie in the same direction but in different columns (e.g. as depicted in Fig. 4 the blue orbitals in the yellow column and the green orbitals in the red column). While keeping the channelling conditions the same but changing the direction of the momentum transfer vector would result in probing different orbital directions in the same column. Usually, a combination of both effects

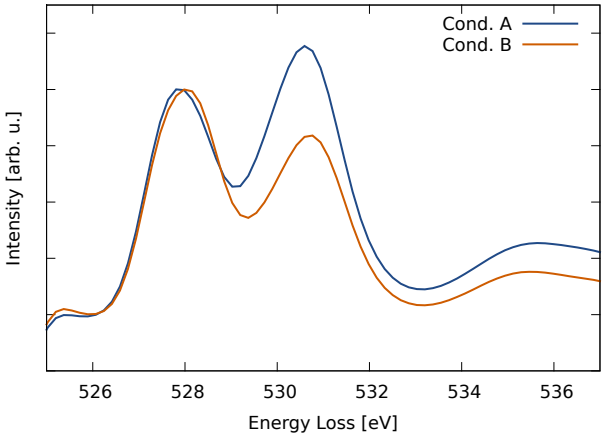

Figure 5: Simulation of the electron energy-loss spectra acquired at different channelling conditions. See Fig. 4 for the definition of conditions "A" and "B".

is observed in the experimental measurements. This is because in the actual experiment, we change the position of the spectrometer entrance aperture (SEA) with respect to the diffraction pattern by shifting the pattern. This shift changes the direction of the outgoing electron wave and therefore changes the channelling conditions. At the same time, the direction of the momentum transfer vector is changed, as it always "points" from the diffraction spots to the position of the SEA. The resulting spectra for the two channelling conditions "A" and "B" are shown in Fig. 5. In the next section, these simulations are compared to actual experimental spectra.

3. Experimental setup

The Rutile sample was prepared in [1 1 0] zone axis using a focused ion beam (FIB) and subsequentially thinned using a GATAN PIPS ion mill. The experiments were conducted using a FEI TECNAI G2 TF20 operated at 200 kV and a FEI TITAN operated at 300 kV. Both instruments have a Gatan GIF Tridiem attached.

The specimen was tilted out of the [1 1 0] zone axis in order to obtain a systematic row condition including the $(1\,\bar{1}\,0)$ diffraction spot. Different channelling conditions were established by shifting the diffraction pattern such that the position of the SEA was changed with respect to the diffraction spots. Due to the quasi Lorentzian behaviour of the DDSC, the intensity of the acquired energy-loss spectra decreases very fast when moving the SEA away from the diffraction spots (Löffler et al., 2011). By increasing the convergence angle, sufficient intensity was gained. As a consequence, the diffraction spots were spread so that the convergence semi-angle was approximately equal to the collection semi-angle (in our experiments about 1 mrad). Under these conditions,

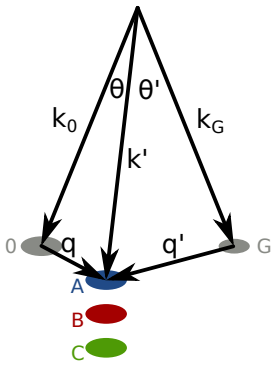

Figure 6: Sketch of the scattering geometry. $\boldsymbol{k}_0$, $\boldsymbol{k}_G$ and $\boldsymbol{k}'$ are momentum vectors, while $\boldsymbol{q}$ and $\boldsymbol{q}'$ are momentum transfer vectors. θ and θ' are the corresponding scattering angles. 0 and G denote Bragg reflections, while "A", "B" and "C" depict the detector positions as they were used in the experiments.

the experimental spectra are still comparable to the simulated ones, for which an incoming plane wave was assumed. A more convergent beam would require a different calculation (e.g. multisclice simulations). A sketch of the scattering geometry is shown in Fig. 6. Three different measurement positions are marked "A" to "C". The SEA was placed a third of the distance between the 0 and the G reflection away from the 0 reflection ($0.3\,\overline{0G}$) and shifted $0.1\,\overline{0G}$, $0.2\,\overline{0G}$ and $0.3\,\overline{0G}$ perpendicular to the systematic row for measurement postitions "A", "B" and "C", respectively. The energy-loss spectra were aquired using a 2.0 mm SEA, a dispersion of 0.2 eV per pixel and an acquisition time of 30 s. The spectral resolution was determined to be 1.0 eV by measuring the full width at half maximum of the zero loss peak. The specimen thickness of about 70 nm was determined using low loss EELS and the Log-ratio method (Egerton, 1996). In the next section, the acquired spectra are compared with the simulations calculated using the experimental parameters.

4. Results and interpretation

Fig. 7 shows, as filled area, the calculated spectra as they arise from the three measurement positions depicted in Fig. 6. In order to facilitate comparison of the three spectra, they are normalised to the maximum of the first peak, which is necessary as the total intensities for the different detector positions are different. It can be seen that by changing the scattering conditions, the relative heights of the peaks at energy-losses of about 528 eV (corresponding to $E_\mathrm{F} + 4$ eV in Fig. 2) and about 531 eV (corresponding to $E_\mathrm{F} + 7$ eV in Fig. 2) can be inverted. As mentioned above, this is due to the change of the direction of the momentum transfer vector $\boldsymbol{q}$ and the subsequent change of the influence of the probed orbitals. At position "A", the $\mathrm{p_y}$ orbitals are probed predominantly while at position "C", the influence of the $\mathrm{p_x}$ and $\mathrm{p_z}$ orbitals is increased. At scattering

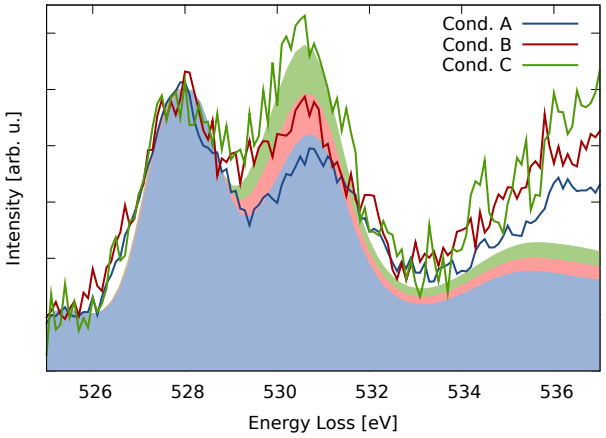

Figure 7: Simulated electron energy-loss spectra calculated using the experimental paramters described in the previous section depicted as filled area. The experimental spectra are plotted in the corresponding colour on top of the simulated ones. The spectra are all normalised to the maximum of the first peak for easier comparison.

condition "B", both orbitals contribute such that the fine-structure exhibits two equally high peaks.

The experimentally acquired spectra are plotted on top of the simulations. The measured spectra are also normalised to the maxima of the first peaks. The inversion of the peak height by using scattering conditions "A" and "C" can be seen clearly. The changes in the peak heights as well as the relative intensities of the peaks around 528 eV and around 531 eV reproduce the calculated behaviour very well.

Thus, ELCE can be used to investigate and interpret the site-specific ionisation edge fine-structure in terms of orbitals and their influence on the energy-loss spectra at different scattering conditions.

5. Conclusion

A combination of two software packages was applied to simulate site-specific electron energy-loss spectra. In the first program, the effects of elastic scattering were treated in a Bloch-wave formalism, while the DFT software package WIEN2k was used to calculate the inelastic scattering process. Comparing the simulations with experimental measurements shows a very good agreement. Furthermore, it was demonstrated on Rutile that using channelling effects and different detector positions, the site-specific investigation of the atomic orbitals is possible by interpreting the changes in the fine-structure of the energy-loss spectra. As the interpretations of the spectra is not straightforward, comparison with simulated spectra is necessary. In contrast to the early years of channelling experiments, these calculations can now be performed at reasonable computa-

tional cost. Moreover, making use of the crystal periodicity, site-specific measurements can be performed to investigate the atoms at different positions in the unit cell without the need for atomic resolution scanning TEM.

Therefore, this technique illustrates new possibilities for chemical and structural analysis in the TEM using ELCE, which is transforming from a rather rarely used method to a powerful application. Possible future applications include the investigation of materials used as catalysts like Vanadium Oxides or MoVTeO.

Acknowledgement

WH, SL and PS acknowledge financial support by the Austrian Science Fund (FWF) under grant number I543-N20. WH thanks M. Stöger-Pollach for fruitful discussions.

References

Blaha, P., Schwarz, K., Madsen, G. K. H., Kvasnicka, D., Luitz, J., 2001. WIEN2k, An Augmented Plane Wave + Local Orbitals Program for Calculating Crystal Properties. Technische Universität Wien, Austria.

Egerton, R. F., 1996. Electron Energy-Loss Spectroscopy in the Electron Microscope, 2nd Edition. Plenum Press New York.

Hébert, C., Schattschneider, P., Rubino, S., Novak, P., Rusz, J., Stöger-Pollach, M., 2008. Magnetic circular dichroism in electron energy loss spectrometry. Ultramicroscopy 108 (3), 277 – 284.

Hetaba, W., Blaha, P., Tran, F., Schattschneider, P., 2012. Calculating energy loss spectra of NiO: Advantages of the modified Becke-Johnson potential. Phys. Rev. B 85 (20), 205108.

Kittel, C., 2006. Einführung in die Festkörperphysik. Oldenbourg Verlag.

Kohl, H., Rose, H., 1985. Theory of Image Formation by Inelastically Scattered Electrons in the Electron Microscope. In: Hawkes, P. W. (Ed.), Advances in Electronics and Electron Physics. Vol. 65 of Advances in Electronics and Electron Physics. Academic Press, pp. 173 – 227.

Krivanek, O., Disko, M., Taftø, J., Spence, J., 1982. Electron energy loss spectroscopy as a probe of the local atomic environment. Ultramicroscopy 9 (3), 249–254.

Laskowski, R., Blaha, P., 2010. Understanding the $L_{2,3}$ x-ray absorption spectra of early 3d transition elements. Phys. Rev. B 82 (20), 205104.

Löffler, S., 2013. Study of real space wave functions with electron energy loss spectrometry. Ph.D. thesis, Vienna University of Technology.

Löffler, S., Ennen, I., Tian, F., Schattschneider, P., Jaouen, N., 2011. Breakdown of the dipole approximation in core losses. Ultramicroscopy 111 (8), 1163–1167.

Löffler, S., Schattschneider, P., 2010. A software package for the simulation of energy-loss magnetic chiral dichroism. Ultramicroscopy 110 (7), 831–835.

Nelhiebel, M., 1999. Effects of crystal orientation and interferometry in electron energy loss spectroscopy. Ph.D. thesis, École Centrale Paris.

Nelhiebel, M., Louf, P.-H., Schattschneider, P., Blaha, P., Schwarz, K., Jouffrey, B., 1999. Theory of orientation-sensitive near-edge fine-structure core-level spectroscopy. Phys. Rev. B 59 (20), 12807–12814.

Nelhiebel, M., Schattschneider, P., Jouffrey, B., 2000. Observation of ionization in a crystal interferometer. Phys. Rev. Lett. 85 (9), 1847–1850.

Rusz, J., Muto, S., Tatsumi, K., 2013. New algorithm for efficient Bloch-waves calculations of orientation-sensitive ELNES. Ultramicroscopy 125, 81 – 88.

Rusz, J., Rubino, S., Schattschneider, P., 2007. First-principles theory of chiral dichroism in electron microscopy applied to 3d ferromagnets. Phys. Rev. B 75 (21), 214425.

Schattschneider, P., Hébert, C., Jouffrey, B., 2001. Orientation dependence of ionization edges in eels. Ultramicroscopy 86 (3-4), 343–353.

Schattschneider, P., Rubino, S., Hébert, C., Rusz, J., Kuneš, J., Novák, P., Carlino, E., Fabrizioli, M., Panaccione, G., Rossi, G., 2006. Detection of magnetic circular dichroism using a transmission electron microscope. Nature 441 (7092), 486–488.

Sorantin, P. I., Schwarz, K., 1992. Chemical bonding in rutile-type compounds. Inorg. Chem. 31 (4), 567–576.

Spence, J., Taftø, J., 1983. ALCHEMI: a new technique for locating atoms in small crystals. Journal of Microscopy 130 (Pt 2), 147–154.

Taftø, J., Krivanek, O. L., 1982. Site-Specific Valence Determination by Electron Energy-Loss Spectroscopy. Phys. Rev. Lett. 48 (8), 560–563.

Taftø, J., Spence, J. C. H., 1982. Crystal Site Location of Iron and Trace Elements in a Magnesium-Iron Olivine by a New Crystallographic Technique. Science 218 (4567), 49–51.

Tatsumi, K., Muto, S., 2009. Local electronic structure analysis by site-selective ELNES using electron channeling and first-principles calculations. J. Phys.: Condens. Matter 21 (10), 104213.

Villars, P., Calvert, L. (Eds.), 1996. Pearson's Handbook of Crystallographic Data for Intermetallic Phases. ASM International.

Williams, D. B., Carter, C. B., 2009. Transmission Electron Microscopy. Springer Science+Business Media.

***Detailed Response to Reviewers**

Dear Editor,
dear Reviewers,

we would like to thank the referees for their extensive reviews and valuable comments.
We would also like to give a short answer on each of the referees' comments and describe what has been changed in the manuscript accordingly.

Reviewer #1:

-) The typos have been corrected.

-) The second paragraph of section 3 has been changed according to the reviewer's comments, such that the experimental setup is formulated more clearly and the effects of the convergence angle when comparing the experimental data to simulations is mentioned.

-) Figure 6 has been changed and now resembles the actual experimental setup.

-) The first paragraphs of section 2 and section 4 have been modified to describe the geometry of the system in a better way. Now, the connection between the Oxygen pDOS, the Orbitals and the arrows in Figures 1 and 4 should be clearer. Furthermore, in section 2 we included a reference to Sorantin and Schwarz 1992, Inorganic Chemistry 3 (4), 567-576, where a detailed description of the bonding situation in Rutile is given. Additionally, electron density plots are shown in the cited manuscript that help to visualise the geometrical situation.

Reviewer #2:

-) The typos have been corrected.

-) We have changed the caption of Figures 3 and 6 according to the reviewer's suggestion. Furthermore, the word "reflex" has been changed to "reflection" where appropriate in the text.

-) The colours of the oxygen atoms in the figures have been changed to red and yellow. Now the types of oxygen atoms should be distinguishable more easily.

-) Figure 6 has been changed and now resembles the actual experimental setup.

Reviewer #3:

-) The last two paragraphs of section 1 have been changed so that the Article Nelhiebel et al. 2000, PRL 85 (9), 1847-1850 is now refered to. In addition, the differences between Nelhiebel's experimental setup and our's has been made clear. Thickness effects have also been mentioned and cited accordingly.

-) In Equation 1, the variable "d" has been changed to "t" and is now defined as sample thickness in the text. Furthermore, equation 1 has been corrected according to the referee's comment.

-) The caption of Figure 4 has been changed to make clear that the direction of the momentum transfer vector in this figure was chosen to resemble an example given in the text.

-) The capital "Q" was a typo and has been changed to a "q". Thus, it is already defined in the text.

-) The reviewer is right with his comment on the energies of the eg and t2g orbitals. The manuscript has been changed as follows: In the first paragraph of section 2 we give a more detailed description of the bonding situation and the orbitals in Rutile. Furthermore, as we probe the oxygen p-states, in the rest of the manuscript we refer to the Oxygen px, py and pz orbitals directly instead of labelling them eg and t2g. This should prevent further misunderstandings.

-) Concerning the last comment of the referee: The mentioned decomposition of the calculated spectra would be quite interesting for sure. However, this is currently not implemented in our simulation program and would require substantial reprogramming. Nevertheless, this will be a task to deal with for our future work. The connection between the measured (and calculated) spectra with the Oxygen px, py and pz orbitals can be seen by comparing Figure 7 and Figure 2. This is now also mentioned in section 4.

Once again, we would like to thank the referees for their thorough reviews.